Relativistic impulse approximation description of polarized proton elastic scattering from polarized ^{13}C

L. Ray, G. W. Hoffmann, M. L. Barlett, and J. D. Lumpe*
Department of Physics, University of Texas at Austin, Austin, Texas 78712

B. C. Clark
Department of Physics, Ohio State University, Columbus, Ohio 43210

S. Hama
Nuclear Research Center, University of Alberta, Edmonton, Alberta, Canada T6G 2J1

R. L. Mercer
IBM Watson Research Laboratories, Yorktown Heights, New York 10598
(Received 20 July 1987)

The elastic scattering of intermediate energy polarized protons from polarized ^{13}C is studied within the framework of the relativistic distorted wave Born approximation using the relativistic impulse approximation to describe the projectile–target nucleon interaction. Sensitivities of observables to (1) the upper and lower components of the valence nucleon wave function, (2) the Lorentz form of the two-body interaction, (3) isoscalar three-vector currents, and (4) the individual strengths of the separate Lorentz terms in the two-body interaction are calculated and discussed. The bound state wave functions for the $1p_{1/2}$ valence neutron used in the calculations are taken from relativistic mean field theory and from traditional, nonrelativistic Woods-Saxon eigenstate solutions. Predictions obtained using either pseudoscalar or pseudovector projectile-nucleon coupling forms are compared. Possible effects on the $\vec{p}+^{13}\vec{C}$ polarized target spin observables due to contributions of the core nucleons to the effective isoscalar three-vector current are discussed and investigated using a simple model. What can be learned from normal (i.e., perpendicular to scattering plane) and transverse (i.e., approximately perpendicular to beam, in the scattering plane) polarized target spin observables, as well as unpolarized $\vec{p}+^{13}C$ elastic scattering observables are discussed. The results suggest that new nuclear structure information, additional effective interaction phenomenology, and further constraints on the Lorentz character of the effective two-body interaction can in principle be obtained from analyses of $\vec{p}+^{13}\vec{C}$ elastic scattering data. Experiments to obtain such data are encouraged.

I. INTRODUCTION

Spin-dependent observables for intermediate energy nucleon-nucleus (NA) scattering processes are invaluable for studying scattering dynamics, nuclear structure, and nucleon-nucleon (NN) effective interactions. For example, pA elastic analyzing power (A_y) and spin-rotation (Q) data were recently used to show the importance of relativistic, virtual ($N\bar{N}$) pair effects in the scattering process.[1–3] The excellent overall agreement between data and predictions of the relativistic impulse approximation–(RIA) Dirac equation model[1–3] contrasted sharply with the results of nonrelativistic (NR) multiple scattering approaches.[4] Spin-dependent observables have also been exploited in inelastic scattering studies at intermediate energies. For example, determinations of $(P-A_y)$,[5] D_{ij},[6] and the spin-flip probability (S) (Ref. 7) have provided useful information with respect to the single and double spin-flip components of the nucleon-nucleon (NN) effective interaction, exchange contributions, spin currents and densities, $M1$ strength, etc.

Preliminary investigations of the possible new physics to be learned from spin observables associated with intermediate energy polarized proton and pion scattering from *polarized nuclear targets* have been made.[8,9] Such studies introduce a new degree of freedom into intermediate energy hadronic physics and open up many new areas for investigation, both experimental and theoretical.

With respect to experimental developments, a number of odd Z (proton number) and/or odd N (neutron number) nuclei can, in principle, be polarized.[10] Recently, a sample of ethylene glycol with 99% ^{13}C enrichment ($C_2H_6O_2$) was polarized to 28% using dynamic nuclear polarization.[11] Experiments[12] which require polarized ^{13}C targets have recently been proposed at the Los Alamos Meson Physics Facility (LAMPF) and will be done over the next several years.

On the theoretical side, scattering data obtained using a polarized ^{13}C target may prove useful for detailed studies of the valence nucleon wave function, further determination of the Lorentz form of the NN effective interaction, and investigation of the strengths and ranges

of those parts of the NN interaction which cannot be readily studied with even-even targets or are poorly determined by analyses of inelastic scattering data.

In anticipation of high quality data from the $\vec{p}+^{13}\vec{C}$ experiment, it is important to develop theoretical models which predict realistic spin observables for polarized odd nuclear targets. In the present work the relativistic impulse approximation–Dirac equation model[1,2] is used to describe $\vec{p}$A elastic scattering, the independent particle model is assumed for the target wave function, and the relativistic distorted wave Born approximation (DWBA) (Ref. 13) is used to generate the scattering amplitude. The model presented in Sec. II is fairly general but is, in many respects, specific to the description of elastic scattering of spin-$\frac{1}{2}$ projectiles from spin-$\frac{1}{2}$ targets. Extension of the RIA model to include other odd targets and other reactions such as (p,p′) or (p,n) is straightforward, however.[14]

In what follows, both the standard RIA interaction[1,2,15] and the recently proposed pseudovector form[16,17] are used to generate predictions for a variety of polarized target elastic spin observables for $\vec{p}+^{13}\vec{C}$ at 500 MeV. RIA predictions for $\vec{p}+^{13}$C differential cross section and analyzing powers at 547 MeV are also given and compared with existing data.[18] Sensitivities of the observables to the $1p_{1/2}$ valence neutron wave function, to the pseudoscalar versus pseudovector Lorentz form for the NN effective interaction, to simple estimates of the core nucleon contribution to the effective isoscalar three-vector current,[19,20] and to the individual strengths of the various terms in the RIA interaction, are explored. Similar relativistic DWBA calculations for $\vec{p}+^{13}\vec{C}$ elastic scattering were presented in Ref. 14. The present work extends considerably both the study in Ref. 14 and the initial plane wave Born approximation calculation in Ref. 9.

The derivation of the elastic scattering amplitude using the proton–odd nucleus relativistic distorted wave Born approximation is given in Sec. II. The model sensitivities and predictions are shown and discussed in Sec. III. A summary and conclusions with respect to the physics potential offered by studies of intermediate energy proton elastic scattering from polarized nuclear targets are given in Sec. IV.

II. THEORETICAL MODEL

The 500 MeV $\vec{p}+^{13}\vec{C}$ elastic scattering observables were calculated using the relativistic impulse approximation for the beam proton–target nucleon interaction[1,15] and a four-component independent particle model for the relativistic target wave function.[21] As yet, a Dirac equation computer program is not available which can accommodate the full relativistic optical potential for an odd target nucleus.[22] The calculations, therefore, use the relativistic distorted wave Born approximation for the valence nucleon ($1p_{1/2}$) portion of the p+^{13}C elastic scattering amplitude. The core contribution to the scattering amplitude (see Sec. II A) is fully handled, with respect to distortions, within the usual RIA model.[1,2] Refinements to the calculations presented here arising from full projectile wave function distortion due to interaction with all 13 nucleons, core deformation effects,[23] multistep processes,[23] particle-hole admixtures in the ^{13}C ground state,[24,25] sophisticated meson exchange models for the NN Lorentz invariant interaction,[17,26] medium effects,[16,27] exchange[16,17] and other nonlocality effects, and target nucleon correlation effects[28] will be considered in the future.

In Sec. II A– the relativistic distorted wave p+^{13}C elastic scattering amplitude is derived, followed in Sec. II B by a delineation of the changes in the model arising when pseudovector rather than pseudoscalar coupling is assumed. In Sec. II C an elementary method for estimating the effects in elastic scattering due to the core contribution to the isoscalar three-vector current is given, while in Sec. II D the calculation of the $\vec{p}+^{13}\vec{C}$ scattering observables is briefly discussed. Finally, Sec. II E gives the various interaction and wave function ingredients in the calculations.

A. p+^{13}C elastic scattering amplitude in the RIA-DWBA

The 500 MeV $\vec{p}+^{13}\vec{C}$ elastic scattering observables were calculated using the first-order RIA optical potential[1,2] given by

$$U^{\rm opt}_{\mu',\mu}=\sum_{i=1}^{A}\langle O_{\mu'}\,|\,t_{0i}\,|\,O_{\mu}\rangle\ , \tag{1}$$

where t_{0i} is the projectile proton-ith target nucleon interaction operator,[1,15]

$$t_{0i}=F_S+F_P\gamma_0^5\gamma_i^5+F_V\gamma_0^\mu\gamma_{i\mu}+F_A\gamma_0^5\gamma_0^\mu\gamma_i^5\gamma_{i\mu}+F_T\sigma_0^{\mu\nu}\sigma_{i\mu\nu}\ . \tag{2}$$

(Projectile and target nucleon are denoted by subscripts 0 and $i=1,2,\ldots,$ respectively.) In Eq. (1) the quantum numbers μ and μ' are the initial and final total angular momentum projection for the target (equal to $\pm\frac{1}{2}$ for ^{13}C), and $|\,0_\mu\rangle$ is the antisymmetrized target wave function given by the independent particle model:

$$|\,O_\mu\rangle=\frac{1}{\sqrt{A!}}\,\mathrm{Det}\prod_{i=1}^{A}u_{\{\alpha\}}(\mathbf{r}_i)\ , \tag{3a}$$

where each member of the set of single particle states, $u_{\{\alpha\}}$, is expressed as

$$u_{nlj\mu}(\mathbf{r})=\begin{bmatrix}\phi_{nlj}(r)\\ -i\boldsymbol{\sigma}\cdot\hat{\mathbf{r}}\lambda_{nlj}(r)\end{bmatrix}Y^\mu_{lj}(\hat{\mathbf{r}})\ . \tag{3b}$$

The large upper component and small lower component are represented by φ and λ, respectively, and $Y^\mu_{lj}(\hat{\mathbf{r}})$ is the spin-angle function. With this target wave function the optical potential separates into the core ($1s_{1/2}$ and $1p_{3/2}$ orbitals) and $1p_{1/2}$ neutron contributions as follows:

$$U^{\rm opt}_{\mu',\mu}(\mathbf{r})=\sum_{\alpha=1}^{A-1}\int d^3r'\bar{u}_\alpha(\mathbf{r}')t(|\mathbf{r}-\mathbf{r}'|)u_\alpha(\mathbf{r}')\delta_{\mu\mu'}$$
$$+\int d^3r'\bar{u}_{n_b l_b j_b \mu'}(\mathbf{r}')t_{\rm pn}(|\mathbf{r}-\mathbf{r}'|)u_{n_b l_b j_b \mu}(\mathbf{r}')$$
$$\equiv U^{\rm core}(\mathbf{r})\delta_{\mu\mu'}+U^{\rm s.p.}_{\mu',\mu}(\mathbf{r}) , \quad (4)$$

where $\bar{u}\equiv u^\dagger\gamma^0$ and n_b, l_b, and j_b are the bound state quantum numbers of the valence nucleon. The core contribution is approximately equal to the p+^{12}C optical potential and includes scalar, timelike vector, and (very small) tensor terms.[29]

In the relativistic distorted wave Born approximation the p+A elastic scattering amplitude is[13,30]

$$f_{m_s'\mu';m_s\mu}(\mathbf{k},\mathbf{k}')\simeq f^{\rm core}_{m_s'm_s}(\mathbf{k},\mathbf{k}')\delta_{\mu'\mu}$$
$$-\frac{m}{2\pi(\hbar c)^2}\langle\chi^{(-)}_{c,\mathbf{k}'m_s'}|U^{\rm s.p.}_{\mu',\mu}|\chi^{(+)}_{c,\mathbf{k}m_s}\rangle , \quad (5)$$

where $f^{\rm core}$ is the exact scattering amplitude for $U^{\rm core}$, m is the proton mass, and $(m_s,\mathbf{k})$ $[(m_s',\mathbf{k}')]$ is the initial (final) spin projection and momentum of the projectile. In Eq. (5) χ_c is the relativistic distorted wave function for the p+^{13}C system arising from $U^{\rm core}$ only. Also in Eq. (5), $\langle\chi^{(-)}|$ implies $\chi^{(-)\dagger}\gamma^0\equiv\bar{\chi}^{(-)}$ in the integral over projectile coordinates.

The contribution to the p+^{13}C elastic scattering amplitude by the valence nucleon was evaluated using standard partial wave expansion techniques. The relativistic distorted waves were expanded as[13,30]

$$\chi^{(+)}_{c,\mathbf{k}m_s}(\mathbf{r})=\left[\frac{E+m}{2m}\right]^{1/2}\sum_{lm_l jm_j}4\pi i^l\begin{bmatrix}\psi_{lj}(kr)Y^{m_j}_{lj}(\hat{\mathbf{r}})\\ i\omega_{lj}(kr)Y^{m_j}_{\tilde{l}j}(\hat{\mathbf{r}})\end{bmatrix}$$
$$\times(lm_l\tfrac{1}{2}m_s|jm_j)Y^*_{lm_l}(\hat{\mathbf{k}}) , \quad (6a)$$

where the relations

$$\boldsymbol{\sigma}\cdot\hat{r}Y^{m_j}_{lj}=-Y^{m_j}_{\tilde{l}j}$$

and

$$\tilde{l}=l\pm1 \quad \text{if } j=l\pm\tfrac{1}{2} \quad (6b)$$

were used for the lower components. From the Dirac equation, $\omega_{lj}(kr)$ is given by

$$\omega_{lj}(kr)=\frac{\hbar c}{E+m+U^{\rm core}_{S,\rm opt}-U^{\rm core}_{0,\rm opt}-U_C}$$
$$\times\left[\frac{d}{dr}-\frac{\langle\boldsymbol{\sigma}\cdot\mathbf{l}\rangle}{r}\right]\psi_{lj}(kr) . \quad (7)$$

In Eq. (7) $U^{\rm core}_{S,\rm opt}$, $U^{\rm core}_{0,\rm opt}$, and U_C are the scalar, timelike vector, and Coulomb parts of the core optical potential, respectively; E is the total projectile energy in the proton-nucleus (pA) center-of-momentum (C.M.) system, and $\langle\boldsymbol{\sigma}\cdot\mathbf{l}\rangle=j(j+1)-l(l+1)-\frac{3}{4}$. The wave function $\bar{\chi}^{(-)}_{c,\mathbf{k}'m_s'}(\mathbf{r})$ is given by[13]

$$\bar{\chi}^{(-)}_{c,\mathbf{k}'m_s'}(\mathbf{r})=\left[\frac{E+m}{2m}\right]^{1/2}\sum_{lm_l jm_j}4\pi i^{-l}(\psi_{lj}(kr)Y^{m_j\dagger}_{lj}(\hat{\mathbf{r}}),i\omega_{lj}(kr)Y^{m_j\dagger}_{\tilde{l}j}(\hat{\mathbf{r}}))(lm_l\tfrac{1}{2}m_s'|jm_j)Y_{lm_l}(\hat{\mathbf{k}}') . \quad (8)$$

Following Shepard, Rost, and Piekarewicz,[13] the NN interaction in Eq. (2) is rewritten as

$$t_{0i}=\sum_{n=1}^{4}[a_n(|\mathbf{r}-\mathbf{r}'|)+b_n(|\mathbf{r}-\mathbf{r}'|)\boldsymbol{\sigma}^{(0)}\cdot\boldsymbol{\sigma}^{(i)}]\Gamma^{(0)}_n\Gamma^{(i)}_n , \quad (9a)$$

where (for $n=1,2,3,4$)

$$\Gamma_1=\begin{bmatrix}1&0\\0&1\end{bmatrix},\quad \Gamma_2=\begin{bmatrix}1&0\\0&-1\end{bmatrix},$$
$$\Gamma_3=\begin{bmatrix}0&1\\1&0\end{bmatrix},\quad \Gamma_4=\begin{bmatrix}0&1\\-1&0\end{bmatrix}, \quad (9b)$$

and, using Eq. (2),

$$a_1=F_S,\quad a_2=F_V,\quad a_3=F_P,\quad a_4=F_A ,$$
$$b_1=2F_T,\quad b_2=-F_A,\quad b_3=2F_T,\quad b_4=-F_V . \quad (9c)$$

In Eq. (9a) the superscripts (0) and (i) refer to the projectile and target nucleon, respectively. Expanding the radial parts of the interaction a_n and b_n in multipoles $T^S_{np}(r,r')$ for $S=0$ and 1, respectively, yields

$$t_{0i}=4\pi\sum_{n=1}^{4}\sum_{S=0,1}\sum_{pq}\frac{T^S_{\rm np}(r,r')}{2p+1}Y_{pq}(\hat{\mathbf{r}})Y^*_{pq}(\hat{\mathbf{r}}')$$
$$\times\sum_{M_S}(-1)^{M_S}\sigma^{(0)}_{S,M_S}\sigma^{(i)}_{S,-M_S}\Gamma^{(0)}_n\Gamma^{(i)}_n . \quad (9d)$$

The σ_{SM_S} are spherical Pauli matrices. Finally, using Eq. (6b), the valence nucleon wave function is expressed as

$$u_{n_b l_b j_b \mu}(\mathbf{r})=\begin{bmatrix}\varphi_{l_b j_b}(r)&Y^\mu_{l_b j_b}(\hat{\mathbf{r}})\\ i\lambda_{l_b j_b}(r)&Y^\mu_{\tilde{l}_b j_b}(\hat{\mathbf{r}})\end{bmatrix} . \quad (10)$$

Equations (4), (6), (8), (9d), and (10) are substituted into Eq. (5) to evaluate the valence nucleon contribution to the $p+^{13}C$ elastic scattering amplitude. In so doing the upper and lower component matrix products for the projectile partial wave functions for each component of the NN interaction are expanded as follows (suppressing functional arguments):

$$(\psi_{l'j'}Y_{l'j'}^{m_j'\dagger}, i\omega_{l'j'}Y_{\bar{l}'j'}^{m_j'\dagger})\Gamma_n^{(0)}\begin{bmatrix}\psi_{lj}Y_{lj}^{m_j}\\ i\omega_{lj}Y_{\bar{l}j}^{m_j}\end{bmatrix}=\sum_{n'=1,2}Y_{l'_{nn'}j'}^{m_j'\dagger}(\hat{\mathbf{r}})X_{ljlj'}^{nn'}(r)Y_{l_{nn'}j}^{m_j}(\hat{\mathbf{r}})\ . \tag{11a}$$

Those for the valence target nucleon are similarly written as

$$(\varphi_{l_bj_b}Y_{l_bj_b}^{\mu'\dagger}, i\lambda_{l_bj_b}Y_{\bar{l}_bj_b}^{\mu'\dagger})\Gamma_n^{(i)}\begin{bmatrix}\varphi_{l_bj_b}Y_{l_bj_b}^{\mu}\\ i\lambda_{l_bj_b}Y_{\bar{l}_bj_b}^{\mu}\end{bmatrix}=\sum_{n''=1,2}Y_{b_{nn''}j_b}^{\mu'\dagger}(\hat{\mathbf{r}}')Z_{l_bj_b}^{nn''}(r')Y_{l_{b_{nn''}}j_b}^{\mu}(\hat{\mathbf{r}}')\ . \tag{11b}$$

The values of $l_{nn'}$, $l'_{nn'}$, $l_{b_{nn''}}$, $l'_{b_{nn''}}$, X, and Z are given in Table I.

The projectile matrix element,

$$\langle\text{proj}\rangle\equiv\sum_{n'=1,2}\int d\hat{\mathbf{r}}\,Y_{l'_{nn'}j'}^{m_j'\dagger}(\hat{\mathbf{r}})Y_{pq}(\hat{\mathbf{r}})\sigma_{SM_S}^{(0)}Y_{l_{nn'}j}^{m_j}(\hat{\mathbf{r}})X_{ljl'j'}^{nn'}(r)\ ,$$

is evaluated using standard Racah algebra together with the relation.

$$\chi_{m_s'}^{\dagger}\sigma_{SM_S}\chi_{m_s}=\hat{S}(\tfrac{1}{2}m_sSM_S\,|\,\tfrac{1}{2}m_s')\ .$$

The resulting expression is

$$\langle\text{proj}\rangle=\sum_{n'=1,2}X_{ljl'j'}^{nn'}(r)\sum_J\frac{1}{\sqrt{2\pi}}(-1)^{j-j'+S-J}\hat{l}_{nn'}\hat{j}\,\hat{p}\,\hat{S}\,\hat{J}$$
$$\times(l_{nn'}0p0\,|\,l'_{nn'}0)(jm_jJ,q+M_S\,|\,j'm_j')(pqSM_S\,|\,J,q+M_S)\begin{Bmatrix}l_{nn'} & \frac{1}{2} & j\\ l'_{nn'} & \frac{1}{2} & j'\\ p & S & J\end{Bmatrix}\ , \tag{12}$$

where $\hat{l}\equiv\sqrt{2l+1}$ and $\{\ \}$ denotes the 9-j symbol. A similar expression results for the valence target nucleon matrix elements.

Substituting these results into Eq. (5) yields, after some further algebra, the following partial wave expansion for the $p+^{13}C$ elastic scattering amplitude:

$$f_{m_s'\mu';m_s\mu}(\hat{\mathbf{k}}')=f_{m_s'm_s}^{\text{core}}(\hat{\mathbf{k}}')\delta_{\mu'\mu}+\sum_{l'}C_{l'}^{m_s'\mu';m_s\mu}Y_{l'm_l'}(\hat{\mathbf{k}}')\ , \tag{13a}$$

TABLE I. Angular momentum quantum numbers and wave functions used in the projectile and valence target neutron matrix elements.

	Values of $(l'_{nn'},l_{nn'})$		Values of $(l'_{b_{nn''}},l_{b_{nn''}})$	
	$n'=1$	$n'=2$	$n''=1$	$n''=2$
$n=1$	(l',l)	$(\bar{l}',\bar{l})$	(l_b,l_b)	$(\bar{l}_b,\bar{l}_b)$
$n=2$	(l',l)	$(\bar{l}',\bar{l})$	(l_b,l_b)	$(\bar{l}_b,\bar{l}_b)$
$n=3$	$(\bar{l}',l)$	$(l',\bar{l})$	$(\bar{l}_b,l_b)$	$(l_b,\bar{l}_b)$
$n=4$	$(\bar{l}',l)$	$(l',\bar{l})$	$(\bar{l}_b,l_b)$	$(l_b,\bar{l}_b)$

	Values of $X_{ljl'j'}^{nn'}$		Values of $Z_{l_bj_b}^{nn''}$	
	$n'=1$	$n'=2$	$n''=1$	$n''=2$
$n=1$	$\psi_{l'j'}\psi_{lj}$	$-\omega_{l'j'}\omega_{lj}$	$\lvert\varphi_{l_bj_b}\rvert^2$	$-\lvert\lambda_{l_bj_b}\rvert^2$
$n=2$	$\psi_{l'j'}\psi_{lj}$	$\omega_{l'j'}\omega_{lj}$	$\lvert\varphi_{l_bj_b}\rvert^2$	$\lvert\lambda_{l_bj_b}\rvert^2$
$n=3$	$i\omega_{l'j'}\psi_{lj}$	$i\psi_{l'j'}\omega_{lj}$	$i\lambda_{l_bj_b}\varphi_{l_bj_b}$	$i\varphi_{l_bj_b}\lambda_{l_bj_b}$
$n=4$	$-i\omega_{l'j'},\psi_{lj}$	$i\psi_{l'j'}\omega_{lj}$	$-i\lambda_{l_bj_b}\varphi_{l_bj_b}$	$i\varphi_{l_bj_b}\lambda_{l_bj_b}$

where

$$C_{l'}^{m_s'\mu';m_s\mu}=-\frac{8\pi(E+m)}{(\hbar c)^2\sqrt{4\pi}}\sum_{Jljj'}I_{ljl'j'J}i^{l-l'}(-1)^{\mu-\mu'+j-j'-J}\hat{j}\hat{j}_b(2J+1)\hat{l}(l'm_l'\tfrac{1}{2}m_s'\mid j',m_l'+m_s')(l0\tfrac{1}{2}m_s\mid jm_s)$$

$$\times(jm_sJ,\mu-\mu'\mid j',m_l'+m_s')(j_b\mu J,\mu'-\mu\mid j_b\mu')\mid_{m_l'=(m_s-m_s')+(\mu-\mu')}, \tag{13b}$$

and the quantization axis was chosen to lie along the incident beam momentum. The radial distorted wave integral is defined according to

$$I_{ljl'j'J}=\int r^2dr\sum_{n=1}^{4}\sum_{n'=1,2}X_{ljl'j'}^{nn'}(r)\hat{l}_{nn'}F_{l_{nn'},l'_{nn'},jj'J}^{nn'}(r)\ , \tag{13c}$$

where

$$F_{l_{nn'},l'_{nn'},jj'J}^{nn'}(r)=\sum_{n''=1,2}\sum_{S=0,1}\sum_{p}(-1)^{p+S}(2S+1)\hat{l}_{b_{nn''}}F_{pnn''}^{S}(r)(l_{nn'}0\mathrm{p}0\mid l'_{nn'}0)$$

$$\times(l_{b_{nn''}}0\mathrm{p}0\mid l'_{b_{nn''}}0)\begin{Bmatrix}l_{nn'}&\frac{1}{2}&j\\ l'_{nn'}&\frac{1}{2}&j'\\ p&S&J\end{Bmatrix}\begin{Bmatrix}l_{b_{nn''}}&\frac{1}{2}&j_b\\ l'_{b_{nn''}}&\frac{1}{2}&j_b\\ p&S&J\end{Bmatrix}, \tag{13d}$$

and the bound state form factor, $F^S_{\mathrm{pnn}''}(r)$, is defined as

$$F_{pnn''}^{S}(r)=\int_0^\infty r'^2dr'T_{np}^{S}(r,r')Z_{l_bj_b}^{nn''}(r')\ . \tag{13e}$$

The required multipoles for $\mathrm{p}+{}^{13}\mathrm{C}$ elastic scattering and the spin transfer components of the NN interaction are listed in Table II. A breakdown of the relevant multipoles, spin, and total angular momentum quantum numbers for each component of the NN interaction, along with the corresponding bound state wave function information required in evaluating Eqs. (13d) and (13e), are given in Table III.

B. Pseudovector coupling

If pseudovector (PV) coupling is assumed for the dominant one-pion exchange portion of the NN interaction, Horowitz[16] and Tjon and Wallace[17] have shown that the predictions of relativistic proton-nucleus scattering models are in much better agreement with data at lower energies, and a more consistent interpretation in terms of meson exchange theory results. This alternative Lorentz coupling form, together with an explicit separation of direct and exchange parts of the NN interaction, while vastly improving agreement with data at energies of a few hundred MeV,[16,17] have negligible consequences on the scalar and timelike vector parts of the optical potential (direct plus exchange parts) at energies ≥ 500 MeV.[16,31] The alternative pseudovector coupling form can, however, directly affect the valence target nucleon contribution to the $\mathrm{p}+{}^{13}\mathrm{C}$ elastic scattering amplitude at any energy; it, therefore, should be considered in the present calculation of polarized target spin observables.

TABLE II. Required multipoles of the NN interaction, $T_{np}^S(r,r')$ (these values apply for $l_b=1$, $j_b=\frac{1}{2}$ only; both $S=0$ and 1 values are implied here).

	$n''=1$	$n''=2$
$n=1$	T_{10}^S,T_{12}^S	T_{10}^S
$n=2$	T_{20}^S,T_{22}^S	T_{20}^S
$n=3$	T_{31}^S	T_{31}^S
$n=4$	T_{41}^S	T_{41}^S

To evaluate this effect, the second term in Eq. (2), $F_P\gamma_0^5\gamma_i^5$, is replaced with[16,17]

$$F_{\mathrm{PV}}\frac{\gamma_0^5(\not{p}_0-\not{p}_0')}{2m}\frac{\gamma_i^5(\not{p}_i-\not{p}_i')}{2m}\ ,$$

where $\not{p}\equiv p^\mu\gamma_\mu$. The evaluation of $\{F_S,F_{\mathrm{PV}},F_V,F_A,F_T\}$ proceeds exactly as in Ref. 15, and owing to the identity

$$\bar{u}_{m_s'}(\mathbf{p}')\gamma^5\frac{(\not{p}-\not{p}')}{2m}u_{m_s}(\mathbf{p})=\bar{u}_{m_s'}(\mathbf{p}')\gamma^5u_{m_s}(\mathbf{p})\ , \tag{14}$$

it is seen that $F_{\mathrm{PV}}=F_P$. In Eq. (14) $u_{m_s}(\mathbf{p})$ is the four-component Dirac spinor with spin projection m_s. The remaining components of the NN interaction are unaffected.

For bound state matrix elements of this new operator the relation

$$\bar{u}_{nlj\mu}\gamma^5\frac{(\not{p}-\not{p}')}{2m}u_{nlj\mu}=\bar{u}_{nlj\mu}\gamma^5\left[1+\frac{U_S}{m}\right]u_{nlj\mu} \tag{15}$$

results, where $u_{nlj\mu}$ is a solution of the bound state Dirac equation:

$$(\not{p}-m-U_B)u_{nlj\mu}=0\ . \tag{16}$$

The binding potential $U_B=U_S+\gamma^0U_V$ contains scalar and timelike vector components. A relation similar to Eq. (15) results for projectile matrix elements, except

TABLE III. Angular momentum quantum numbers[a] and corresponding valence nucleon wave function information for the $p_{1/2} \rightarrow p_{1/2}$ elastic transition for each Lorentz component of the NN effective interaction.

n	Force description	S	p	J	Proportional valence nucleon structure
1	Scalar	0	0	0	$\|\varphi\|^2 - \|\lambda\|^2$
2	Timelike vector	0	0	0	$\|\varphi\|^2 + \|\lambda\|^2$
3	Pseudoscalar	0	1	1	$\varphi\lambda$
4	Timelike axial vector	0	1	1	(Vanishes)
1	Tensor_{ij}	1	0	1	$\|\varphi\|^2 + 3\|\lambda\|^2$
		1	2	1	$\|\varphi\|^2$
2	Axial three-vector	1	0	1	$\|\varphi\|^2 - 3\|\lambda\|^2$
		1	2	1	$\|\varphi\|^2$
3	Tensor_{0i}	1	1	0	$\varphi\lambda$
		1	1	1	(Vanishes)
4	Three-vector	1	1	0	(Vanishes)
		1	1	1	$\varphi\lambda$

[a] S and p denote the spin and multipole quantum numbers of the two-body interaction, respectively, in Eq. (9d) in the text. J is the total angular momentum transfer for the target nucleon introduced in Eqs. (13b) and (13d).

that the factor $(1+U^{\text{core}}_{S,\text{opt}}/m)$ is obtained. Therefore, for pseudovector coupling, the $S=0$, $n=3$ bound state form factor $F^S_{\text{pnn}''}(r)$ in Eq. (13e) is replaced with

$$F^0_{p3n''}(r) = \left[1+\frac{U^{\text{core}}_{S,\text{opt}}(r)}{m}\right] \int_0^\infty r'^2 dr' T^0_{3p}(r,r') Z^{3n''}_{l_b j_b}(r') \times \left[1+\frac{U_S(r')}{m}\right] . \quad (17)$$

Results of calculations using this $\gamma^5 \not{q}/2m$ form are discussed in Sec. III.

C. Isoscalar three-vector currents

A long-standing failure of relativistic nuclear structure models has been the large overestimate of the isoscalar magnetic moments of odd nuclei[32] due to enhancement of the lower component of the relativistic wave function of the odd nucleon (due to the strong scalar and vector binding potentials). This difficulty has been addressed by Furnstahl and Serot,[19] and by McNeil *et al.*[20] The authors in Ref. 19 utilize a relativistic quantum field theoretical approach[33] and calculate, in first-order perturbation theory, the response of the core to the presence of the single valence nucleon; McNeil *et al.*[20] assume a Landau-Migdal quasiparticle approach to relativistic nuclear matter. Both[19,20] show that the isoscalar three-vector current of the odd A target (even-even core plus one particle) can be represented by an effective single particle valence nucleon three-vector current in which enhancement of the lower component of the valence nucleon is suppressed to the weak binding potential (so-called "nonrelativistic" limit) value. These results are valid only for scattering from infinite nuclear matter at zero-momentum transfer. How the core response affects the isoscalar three-vector current at nonzero momentum transfer in finite nuclei has recently been studied[34] and further analysis of this effect is in progress. In the meantime, for the purposes of this sensitivity study, we assume a simple model for the quenching of the isoscalar three-vector current enhancement in order to provide an estimate of possible effects on the $p+{}^{13}C$ elastic scattering spin observables. The sensitivity of the predicted polarized target spin observables to this quenching effect (see Sec. III) provides an impetus for further experimental and theoretical studies of this scattering system.

In the present model, the isoscalar portion of $F^1_{p4n''}(r)$ in Eq. (13e) is computed assuming the weak relativistic binding potential (WRBP) limit for the lower component, $\lambda^{\text{WRBP}}_{n_b l_b j_b}(r)$, obtained from the solution of the bound state Dirac equation with vanishing binding potentials, and is given by

$$\lambda^{\text{WRBP}}_{n_b l_b j_b}(r) = \frac{\hbar c}{2m - \epsilon_{n_b l_b j_b}} \left[\frac{d}{dr} - \frac{\langle \sigma \cdot l_b \rangle}{r}\right] \varphi_{n_b l_b j_b}(r) , \quad (18)$$

where $\epsilon_{n_b l_b j_b}$ is the valence nucleon binding energy. The remaining form factors and the isovector portion of $F^1_{p4n''}(r)$ are computed as before using a relativistic $\lambda(r)$.

D. Calculation of scattering observables

It is convenient to recast the p+^{13}C elastic scattering amplitude into a more conventional form.[35] This is achieved by requiring that at each value of momentum transfer.

$$f_{m_s'\mu';m_s\mu}=\chi^{\dagger(0)}_{m_s'}\chi^{\dagger(1)}_{\mu'}\tfrac{1}{2}[(a+b)+(a-b)\sigma_n^{(0)}\sigma_n^{(1)} +(c+d)\sigma_s^{(0)}\sigma_s^{(1)}+(c-d)\sigma_l^{(0)}\sigma_l^{(1)} +(e+f)\sigma_n^{(0)}+(e-f)\sigma_n^{(1)}]\chi^{(1)}_{\mu}\chi^{(0)}_{m_s}\,, \tag{19}$$

where (0) and (1) refer to the projectile and target nucleus, respectively, χ denotes a Pauli spinor, $\sigma_x\equiv\boldsymbol{\sigma}\cdot\hat{\mathbf{x}}$, $\hat{\mathbf{n}}=(\mathbf{k}\times\mathbf{k}')/|\mathbf{k}\times\mathbf{k}'|$, $\hat{\boldsymbol{l}}=(\mathbf{k}+\mathbf{k}')/|\mathbf{k}+\mathbf{k}'|$, and $\hat{\mathbf{s}}=(\mathbf{k}'-\mathbf{k})/|\mathbf{k}'-\mathbf{k}|$. All scattering observables required to predict the $\hat{\mathbf{n}}$, $\hat{\mathbf{s}}$, and $\hat{\boldsymbol{l}}$ polarizations of the scattered protons were evaluated for all possible spin orientations of the beam and target. Observables which depend on the polarization of the recoil ^{13}C were not considered. The notation for observables is that of Ref. 35 where, for X_{ijkl}, i, j, k, and l refer to the measured spin orientation of the scattered proton, recoil target (not used), beam proton, and target ^{13}C, respectively. The observables in the p+^{13}C center-of-momentum (C.M.) frame in terms of the $(\hat{\mathbf{s}},\hat{\mathbf{n}},\hat{\boldsymbol{l}})$ coordinate system were evaluated by standard methods and are given in Table IV in terms of the $\{a,b,c,d,e,f\}$ amplitudes. Observables with spin components in the directions $\hat{\mathbf{s}}$, $\hat{\mathbf{n}}$, and $\hat{\boldsymbol{l}}$ are denoted by subscripts S, N, and L, respectively, in Table IV, in the figures, and in the discussion which follows. The observables shown in the figures are C.M. quantities.

TABLE IV. Summary of $\vec{\mathrm{p}}+^{13}\vec{\mathrm{C}}$ elastic scattering observables.

$d\sigma/d\Omega$	$=\frac{1}{2}(\lvert a\rvert^2+\lvert b\rvert^2+\lvert c\rvert^2+\lvert d\rvert^2+\lvert e\rvert^2+\lvert f\rvert^2)$
σP	$=\mathrm{Re}(a^*e+b^*f)$
A_{00N0}	$=P$
σD_{N0N0}	$=\frac{1}{2}(\lvert a\rvert^2+\lvert b\rvert^2-\lvert c\rvert^2-\lvert d\rvert^2+\lvert e\rvert^2+\lvert f\rvert^2)$
σD_{L0S0}	$=\mathrm{Im}(b^*e+a^*f)$
D_{S0L0}	$=-D_{L0S0}$
σD_{S0S0}	$=\mathrm{Re}(a^*b+c^*d-e^*f)$
σD_{L0L0}	$=\mathrm{Re}(a^*b-c^*d-e^*f)$
σA_{00NN}	$=\frac{1}{2}(\lvert a\rvert^2-\lvert b\rvert^2-\lvert c\rvert^2+\lvert d\rvert^2+\lvert e\rvert^2-\lvert f\rvert^2)$
σA_{000N}	$=\mathrm{Re}(ae^*-bf^*)$
M_{N0NN}	$=A_{000N}$
σK_{N00N}	$=\frac{1}{2}(\lvert a\rvert^2-\lvert b\rvert^2+\lvert c\rvert^2-\lvert d\rvert^2+\lvert e\rvert^2-\lvert f\rvert^2)$
σM_{L0LN}	$=\mathrm{Re}(b^*e-a^*f)$
M_{S0SN}	$=M_{L0LN}$
σM_{L0SN}	$=-\mathrm{Im}(a^*b+c^*d+f^*e)$
σM_{S0LN}	$=\mathrm{Im}(a^*b-c^*d-e^*f)$
σK_{L00S}	$=\mathrm{Im}(c^*e+d^*f)$
σA_{00LS}	$=-\mathrm{Im}(d^*e+c^*f)$
σK_{S00S}	$=\mathrm{Re}(a^*c+b^*d)$
σM_{L0NS}	$=-\mathrm{Im}(a^*c+b^*d)$
σA_{00SS}	$=\mathrm{Re}(a^*d+b^*c)$
σM_{N0LS}	$=\mathrm{Im}(a^*d+b^*c)$
σM_{N0SS}	$=\mathrm{Re}(de^*+cf^*)$
σM_{S0NS}	$=\mathrm{Re}(ce^*+df^*)$
σM_{L0NL}	$=\mathrm{Re}(c^*e-d^*f)$
σM_{N0LL}	$=-\mathrm{Re}(d^*e-c^*f)$
A_{00SL}	$=-A_{00LS}$
σK_{L00L}	$=\mathrm{Re}(a^*c-b^*d)$
σM_{S0NL}	$=\mathrm{Im}(a^*c-b^*d)$
σA_{00LL}	$=-\mathrm{Re}(a^*d-b^*c)$
σM_{N0SL}	$=\mathrm{Im}(a^*d-b^*c)$
σK_{S00L}	$=\mathrm{Im}(ce^*-df^*)$

E. Ingredients in the calculations

The distorted waves and the core contribution to the full scattering amplitude were computed as follows. The SP82 NN phase shift solution of Arndt[36] provided the on-shell amplitudes used to generate the five t matrices in Eq. (2); the transformation from Pauli two-component spin matrix representation to Dirac four-component γ-matrix representation and Breit frame relativistic kinematics was done as described in Refs. 2 and 15. The proton-vector density due to the $1s_{1/2}$ and $1p_{3/2}$ core wave functions was determined from the empirical ^{12}C charge density[37] by unfolding the single nucleon electric form factor and correcting for the nucleon magnetic form factors.[38,39] The core neutron vector density was parametrized as[2]

$$\rho^{\mathrm{n}}_{V,\mathrm{core}}(r)=\rho^{\mathrm{n}}_{V,\mathrm{core}}(r)\,|_{\mathrm{theory}} +\left[\frac{\rho_0'}{1+\exp[(r-c)/z]} -\frac{\rho_0}{1+\exp[(r-c_0)/z_0]}\right], \tag{20}$$

where ρ_0 and ρ_0' normalized each Fermi function to six neutrons, and c_0 and z_0 were selected to reproduce the surface region of $\rho^{\mathrm{n}}_{V,\mathrm{core}}(r)\,|_{\mathrm{theory}}$, given by[2]

$$\rho^{\mathrm{n}}_{V,\mathrm{core}}(r)\,|_{\mathrm{theory}}=\rho^{\mathrm{p}}_{V,\mathrm{core}}(r)+[\rho_{\mathrm{n}}(r)-\rho_{\mathrm{p}}(r)]_{\mathrm{HFB}}\,. \tag{21}$$

The empirical proton-vector core density is $\rho^{\mathrm{p}}_{V,\mathrm{core}}(r)$, while the proton and neutron densities, labeled HFB, are the ^{12}C mean field Hartree-Fock-Bogoliubov (HBF) distributions of Dechargé and Gogny.[40] The reference density parameters, c_0 and z_0, are 2.265 and 0.36 fm, respectively. The variable surface geometry parameters, c and z, were adjusted to optimize the fit of the RIA model to preliminary 500 MeV p+^{12}C elastic differential cross section data.[41] Values of 2.243 and 0.34 fm for c and z, respectively, were obtained. The scalar densities for the core were taken as[2]

$$\rho^{(i)}_{S,\mathrm{core}}(r)=\rho^{(i)}_{V,\mathrm{core}}(r)+[\rho^{(i)}_S(r)-\rho^{(i)}_V(r)]_{\mathrm{RMFT}}\,, \tag{22}$$

where (i) represents protons or neutrons and the densities in square brackets are the relativistic mean field theory (RMFT) ^{12}C core densities of Horowitz and Serot.[21] The core distorted waves χ_c and the core con-

tribution to the $p+^{13}C$ scattering amplitude $f^{\rm core}_{m_s' m_s}(\hat{\mathbf{k}}')$, were then computed using the RIA-Dirac equation model of Ref. 2 and $p+^{13}C$ relativistic kinematics.

For numerical evaluation of the valence neutron contribution to the scattering amplitude, each term in the Lorentz invariant interaction was parametrized by a sum of five Yukawa functions with ranges corresponding to physical meson masses.[42] This was done to enable numerical convenience in computing the multipoles $T^S_{np}(r,r')$ and to provide an analytic extrapolation of the amplitudes to large q^2. A variety of forms were assumed for the $1p_{1/2}$ neutron wave function, including the RMFT forms for φ and λ from Ref. 21, a nonrelativistic bound state for φ, and both the weak relativistic binding potential limit for λ of Eq. (18) and a relativistic single particle Dirac (RSPD) equation bound state form for $\lambda_{1p_{1/2}}(r)$ given by

$$\lambda^{\rm RSPD}_{nlj}(r)=\frac{\hbar c}{2m-\epsilon_{nlj}+U_S(r)-U_V(r)} \times\left[\frac{d}{dr}-\frac{\langle\sigma\cdot l\rangle}{r}\right]\varphi_{nlj}(r)\ . \tag{23}$$

which was obtained from solution of the Dirac equation. In Eq. (23) $U_S(r)$ and $U_V(r)$ are single particle binding potentials. Calculations employing the weak binding limit lower component $1p_{1/2}$ wave function demonstrate the model sensitivity to the large relativistic binding potentials. In this work, to simplify sensitivity studies, we chose the simple parametrizations for U_S and U_V given by

$$U_S(r)=\frac{V_S}{1+\exp[(r-c_S)/z_S]}$$

and (24)

$$U_V(r)=\frac{V_V}{1+\exp[(r-c_V)/z_V]}\ ,$$

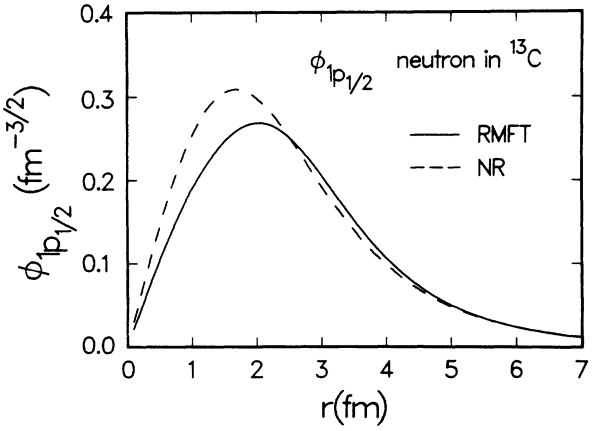

FIG. 1. Single particle bound state radial wave function for a $1p_{1/2}$ neutron in ^{13}C. Solid curve corresponds to the upper component of the RMFT wave function from Ref. 21. The dashed curve is the Woods-Saxon eigenstate of the single particle Schrödinger equation.

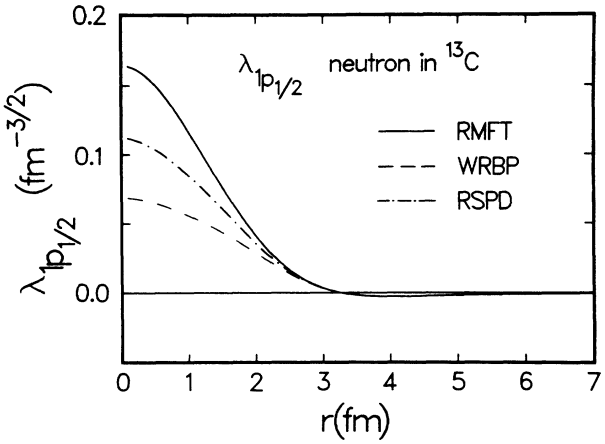

FIG. 2. Lower components of the $1p_{1/2}$ neutron single particle wave function in ^{13}C. The RMFT value (see Ref. 21) is given by the solid curve. The dashed and dashed-dotted curves denote those wave functions computed from the single particle Dirac equation as in Eqs. (18) and (23), respectively.

where V_S, c_S, z_S, V_V, c_V, and z_V were assumed to have values of -400 MeV, 1.95 fm, 0.52 fm, 350 MeV, 1.95 fm, and 0.52 fm, respectively. These strengths are typical of those of low energy scalar and vector optical potentials.[43,44] The different models for $\varphi_{1p_{1/2}}$ and $\lambda_{1p_{1/2}}$ are shown in Figs. 1 and 2, respectively.

III. RESULTS AND DISCUSSION

In the following, model sensitivities to the lower component of the valence nucleon wave function are examined, various predictions of $\vec{p}+^{13}\vec{C}$ spin observables are shown, predictions of 547 MeV $\vec{p}+^{13}C$ differential cross section and analyzing powers are shown, pseudovector coupling effects and quenched isoscalar three-vector current effects are examined, and sensitivities of observables to the individual components of the NN interaction are studied.

We first consider the valence neutron contributions to unpolarized target observables. Figure 3 compares $d\sigma/d\Omega$, P (polarization), D_{LOSO} [essentially $-Q(\theta)$ at small momentum transfer, Ref. 45], D_{SOSO}, and D_{NONO} for 500 MeV $\vec{p}+^{13}C$ using the full amplitude in Eq. (13a) (solid curves) and predictions obtained using just the core amplitude, $f^{\rm core}_{m_s' m_s}(\hat{\mathbf{k}}')$ (dashed curves). For the full $\vec{p}+^{13}C$ case, the standard RIA interaction with pseudoscalar coupling was used along with the RMFT results for $\varphi_{1p_{1/2}}$ and $\lambda_{1p_{1/2}}$. Isoscalar three-vector currents were computed assuming full enhancement of $\lambda_{1p_{1/2}}$. In the following discussion this $p+^{13}C$ calculation will be referred to as the "standard RIA calculation."

Generally, the valence neutron effects are very small; the structure features show slight inward shifts to smaller angles owing to the small increase in overall size due to the additional nucleon. The departure of D_{NONO} from unity indicates the presence of total angular momentum transfer $J=1$ contributions to the elastic scattering

channel. These arise from the valence neutron scattering amplitude through the $J=1$ parts (primarily the pseudoscalar) of the NN interaction (see Table III). We also note that for each observable shown in Fig. 3, other than D_{NONO}, little sensitivity to different models for $\varphi_{1p_{1/2}}$ or $\lambda_{1p_{1/2}}$ exists. These observables are also insensitive to the choice of pseudoscalar or pseudovector coupling, quenching of the isoscalar three-vector current, and parts of the NN interaction other than the scalar and timelike vector terms. Nonetheless, such data are required because they will help determine the core scattering amplitude.

In Fig. 4, standard RIA model predictions are compared with cross section and analyzing power data[18] for 547 MeV $\vec{p}+{}^{13}C$ (NN amplitudes evaluated at 547 MeV were used). The curves qualitatively describe the data; however, inclusion of core deformation and multistep effects would probably improve the agreement. The results shown in Figs. 3 and 4 suggest that a successful

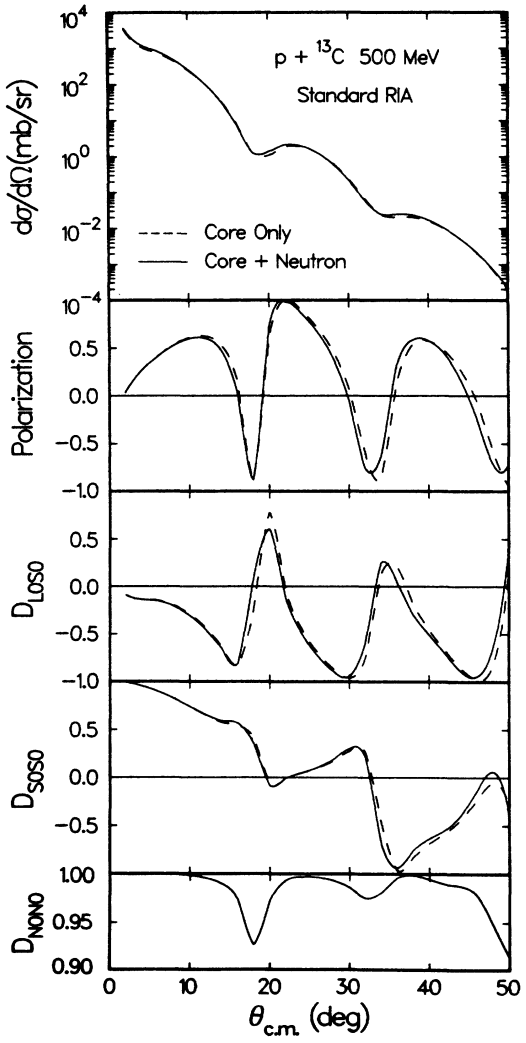

FIG. 3. Standard RIA predictions (see text) for unpolarized target observables for 500 MeV $\vec{p}+{}^{13}C$ (solid curves) compared to the observables computed assuming only the contribution of the core nucleons (dashed curves).

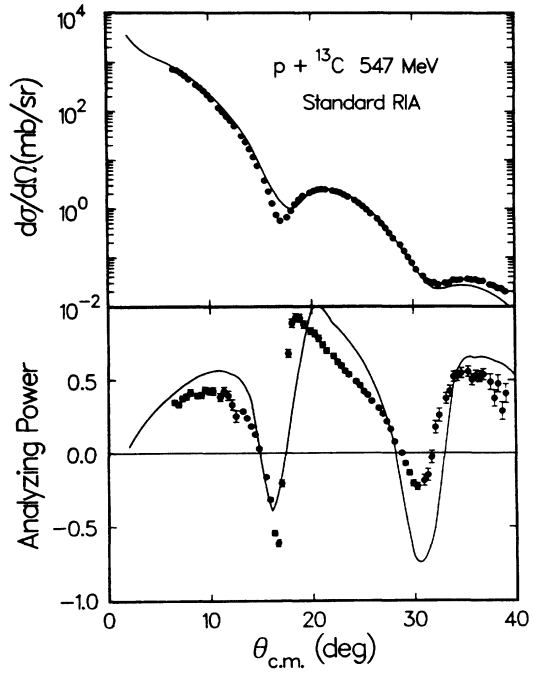

FIG. 4. Standard RIA elastic scattering differential cross section and analyzing power predictions (see text) compared with data for 547 MeV $\vec{p}+{}^{13}C$.

description of the unpolarized target observables mainly requires a realistic treatment of the core portion of the scattering amplitude; the theoretical treatment of the valence neutron contribution to the scattering amplitude is of lesser importance.

The discussion of polarized target observables[35] begins with an investigation of their dependence upon the various terms in the Lorentz invariant NN amplitudes. Typical of the $\hat{n}$-target results are the analyzing powers, A_{000N} and A_{00NN}, shown in Fig. 5 (note the expanded scale used here and in other figures showing polarized target spin observables). The standard RIA results are indicated by the solid curves, while the standard RIA results obtained using only the pseudoscalar (PS), tensor, axial vector, or vector interactions individually for the valence neutron contribution to the scattering amplitude are indicated by the dashed, short-dashed-dot, long-dashed-dot, and dotted curves, respectively. We see that the spacelike vector interaction (associated with the three-vector current) gives the largest contribution to A_{000N} and A_{00NN}, the axial vector and tensor contributions are also important, and the pseudoscalar contribution is negligible. The results for analyzing powers A_{00LS} and A_{00SS} ($\hat{s}$-type polarized target) are shown in Fig. 6, where the meaning of the curves is the same as in Fig. 5. Here, however, the pseudoscalar interaction gives the largest contribution, the tensor contribution is non-negligible, and the axial vector and three-vector contributions are small. For A_{00LL} ($\hat{l}$-type polarized target) Fig. 7 indicates that the axial-vector and tensor contributions are dominant; the pseudoscalar and vector contributions are small. Since the spacelike vector and pseudoscalar interactions dominate the valence neutron

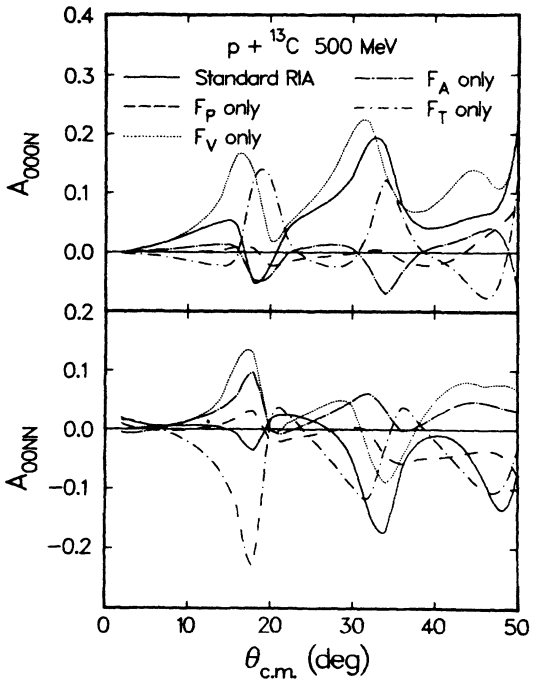

FIG. 5. $\hat{n}$-type polarized target spin observable predictions for 500 MeV $\vec{p}+^{13}\vec{C}$ using the standard RIA model (see text) assuming for the valence neutron contribution the full RIA interaction (solid curves), the pseudoscalar interaction only (dashed curves), the vector interaction only (dotted curves), the axial vector interaction only (long-dashed-dotted curves), and the tensor interaction only (short-dashed-dotted curves). Note the expanded scale used for the polarized target spin observables.

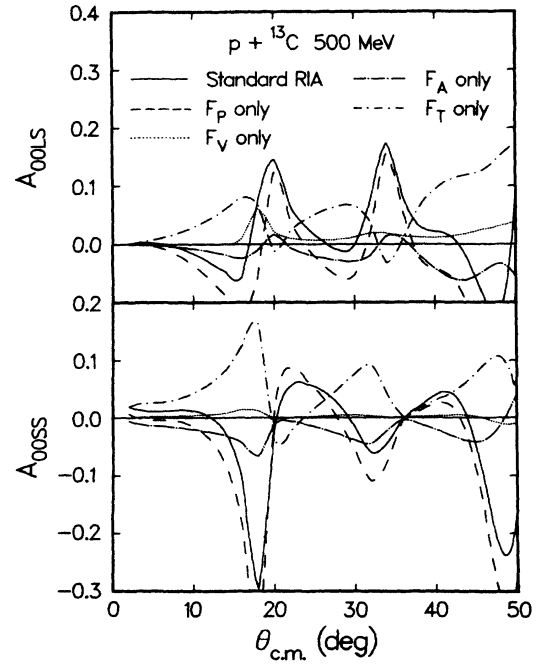

FIG. 6. Same as in Fig. 5, except for an $\hat{s}$-type polarized target.

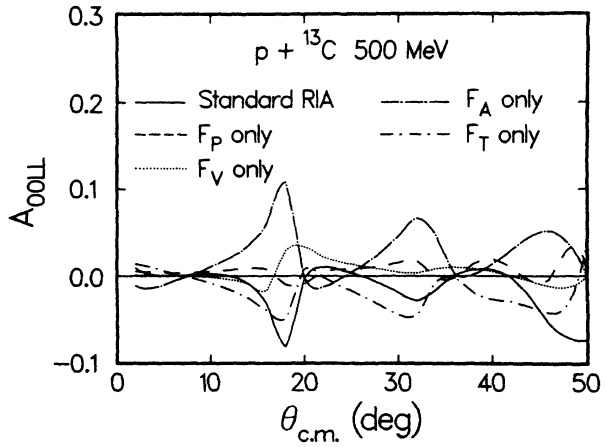

FIG. 7. Same as in Fig. 5, except for an $\hat{l}$-type polarized target.

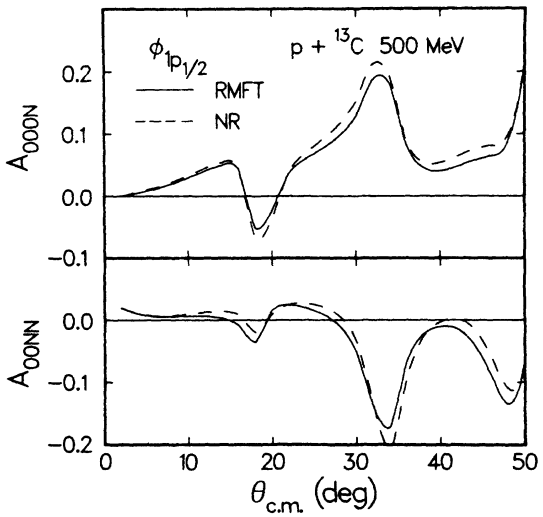

FIG. 8. RIA predictions for A_{000N} and A_{00NN} assuming either the RMFT (Ref. 21) (solid curves) or the Schrödinger equation eigenstate (dashed curves) for the upper component of the $1p_{1/2}$ valence neutron wave function.

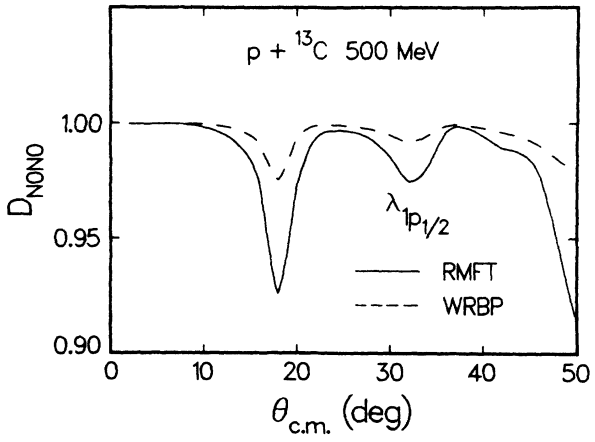

FIG. 9. Predicted sensitivity in D_{N0N0} to $\lambda_{1p_{1/2}}(r)$ in the RIA model. The two curves were generated assuming either the RMFT value (Ref. 21) for $\lambda_{1p_{1/2}}$ (solid curve), or the weak binding potential limit from Eq. (18) (dashed curve) as explained in the text. Note the expanded scale.

contributions to the $\hat{n}$- and $\hat{s}$-type polarized target spin observables, we see from Table III that the valence nucleon structure enters the calculation as the product $\varphi_{1p_{1/2}}(r)\lambda_{1p_{1/2}}(r)$; thus these observables are almost directly proportional to relativistic enhancement of $\lambda_{1p_{1/2}}(r)$ due to the strong scalar and timelike vector binding potentials in the nuclear medium.[21,33] The dependence of A_{00LL} upon $|\varphi|^2$, $|\lambda|^2$, and $\varphi\lambda$ renders it less likely to demonstrate qualitative sensitivity to $\lambda_{1p_{1/2}}(r)$. We point out, however, that these various levels of model sensitivity to $\lambda_{1p_{1/2}}(r)$ are strongly dependent on the assumed Lorentz coupling form and on the estimated core contribution to the isoscalar three-vector current (see the following discussion). The results in Figs. 5–7 may serve to be useful for investigating the contributions of the various invariant NN amplitudes to $\hat{n}$-, $\hat{s}$-, and $\hat{l}$-type polarized target spin observables.

We now examine polarized target observable sensitivity to the valence neutron wave function (in the standard RIA model). The observables are directly dependent on $\varphi_{1p_{1/2}}(r)$; however, for a reasonable range of variation, such as that given by the differences between the RMFT wave function and the nonrelativistic Woods-Saxon bound state wave function (see Fig. 1), small effects are seen. Typical sensitivities are shown in Fig. 8 for A_{000N} and A_{00NN}, where the solid and dashed curves correspond to the standard RIA calculations assuming the RMFT $\varphi_{1p_{1/2}}(r)$ and the NR $\varphi_{1p_{1/2}}(r)$, respectively. Sensitivity to other nuclear structure effects (e.g., particle-hole admixtures[24,25]) could possibly be greater.

Sensitivity to $\lambda_{1p_{1/2}}(r)$ is shown in Fig. 9 for D_{NONO}, and in Figs. 10–12 for some of the polarized target observables. The solid curves are standard RIA results

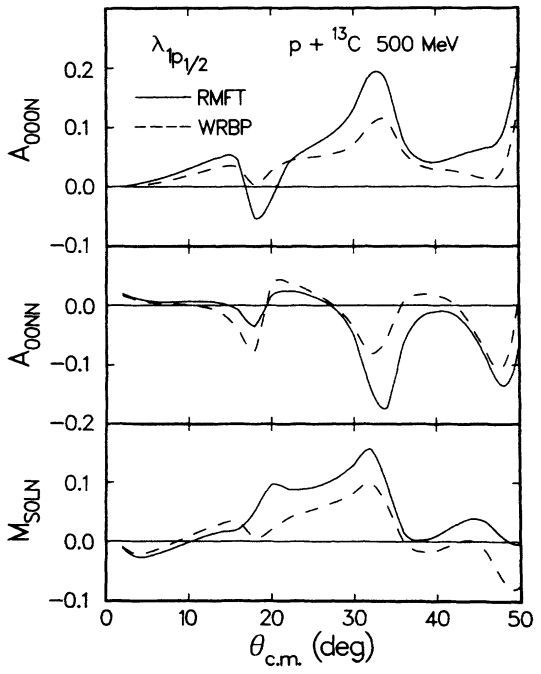

FIG. 10. Same as in Fig. 9, except for A_{000N}, A_{00NN}, and M_{SOLN}.

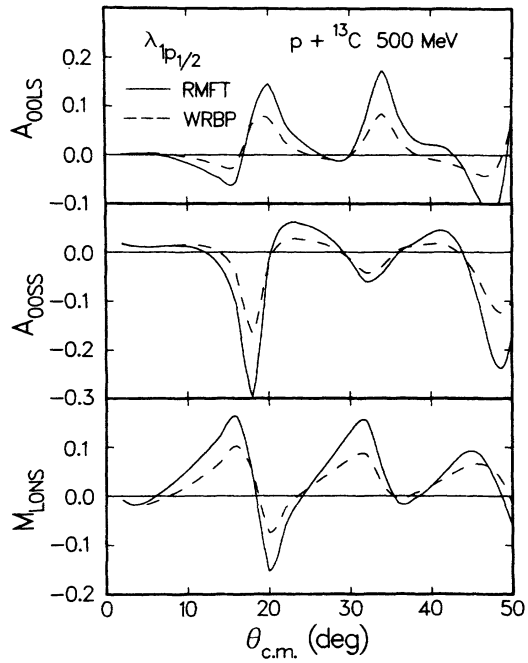

FIG. 11. Same as in Fig. 9, except for A_{00LS}, A_{00SS}, and M_{LONS}.

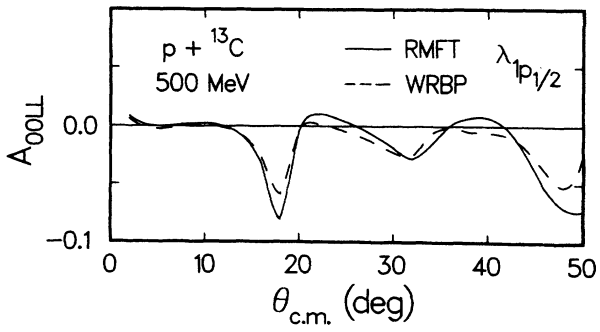

FIG. 12. Same as in Fig. 9, except for A_{00LL}.

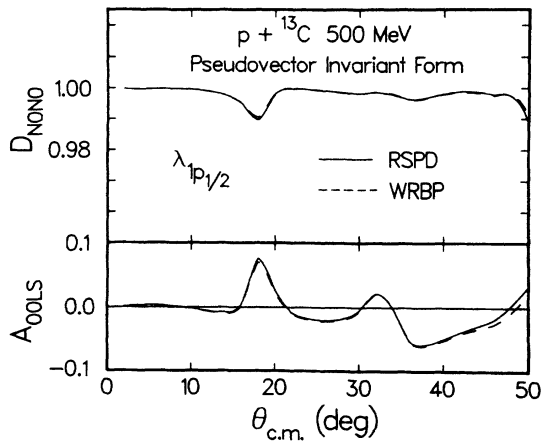

FIG. 13. Demonstration of the predicted loss of sensitivity to $\lambda_{1p_{1/2}}(r)$ for D_{NONO} and A_{00LS} when pseudovector rather than pseudoscalar coupling is assumed in the RIA interaction. Solid and dashed curves correspond to $\lambda_{1p_{1/2}}$ from Eqs. (23) and (18) in the text, respectively.

where the RMFT value for $\lambda_{1p_{1/2}}(r)$ is assumed; the dashed curves display the results of similar calculations using $\lambda^{\mathrm{WRBP}}_{1p_{1/2}}(r)$ discussed in Sec. II [see Eq. (18)] and shown in Fig. 2. The level of sensitivity to $\lambda_{1p_{1/2}}(r)$ is moderate for D_{NONO} and the $\hat{n}$- and $\hat{s}$-target spin observables. This sensitivity is about one-half of that estimated in Ref. 9 using the plane wave Born approximation.

However, when pseudovector coupling is assumed, as discussed in Sec. II B, the model sensitivity to $\lambda_{1p_{1/2}}$ for D_{NONO} and the $\hat{s}$-type polarized target spin observables is essentially eliminated as shown in Fig. 13. For these calculations the Dirac equation bound state $\lambda^{\mathrm{RSPD}}_{1p_{1/2}}$ [see Eq. (23)] and $\lambda^{\mathrm{WRBP}}_{1p_{1/2}}$ were used alternately. The sensitivity to $\lambda_{1p_{1/2}}(r)$ in the $\hat{n}$-target observables remains, since the pseudoscalar contribution to these observables is negligible. If we additionally adopt *both* the pseudovector coupling form and the estimated core contribution to the isoscalar three-vector current as in Sec. II C, the remaining sensitivity to $\lambda_{1p_{1/2}}(r)$ in the $\hat{n}$-type target observables is also eliminated as shown in Fig. 14. Here also $\lambda_{1p_{1/2}}(r)$ was obtained either from Eq. (18) or (23). Therefore, for the theoretically preferred pseudovector model in which the core contributes to the isoscalar three-vector current, very little sensitivity to relativistic enhancement of the valence nucleon lower component is predicted for any elastic scattering observable. Mixing of pseudoscalar and pseudovector interaction contributions, and variations (from that assumed here) in the core contribution to the effective isoscalar three-vector current at finite momentum transfer for finite nuclei (see Sec. II C and Ref. 34) might restore some model sensitivity to $\lambda_{1p_{1/2}}(r)$.

It is also worthwhile to directly investigate the model sensitivity to pseudovector versus pseudoscalar coupling. Results are shown in Fig. 15 for D_{NONO}, A_{00LS}, and A_{00SS}, where the solid (dashed) curves correspond to pseudoscalar (pseudovector) coupling, and the relativistic single particle bound state wave function of Eq. (23) is assumed for $\lambda_{1p_{1/2}}(r)$. Considerable sensitivity to the choice of Lorentz form is evident in each case shown.

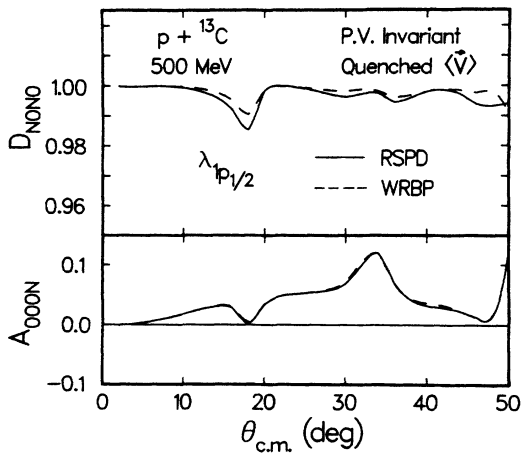

FIG. 14. Demonstration of the predicted loss of sensitivity to $\lambda_{1p_{1/2}}(r)$ for D_{NONO} and A_{000N} when pseudovector coupling and core suppression of the isoscalar three-vector current are both assumed. Solid and dashed curves correspond to $\lambda_{1p_{1/2}}$ from Eqs. (23) and (18) in the text, respectively.

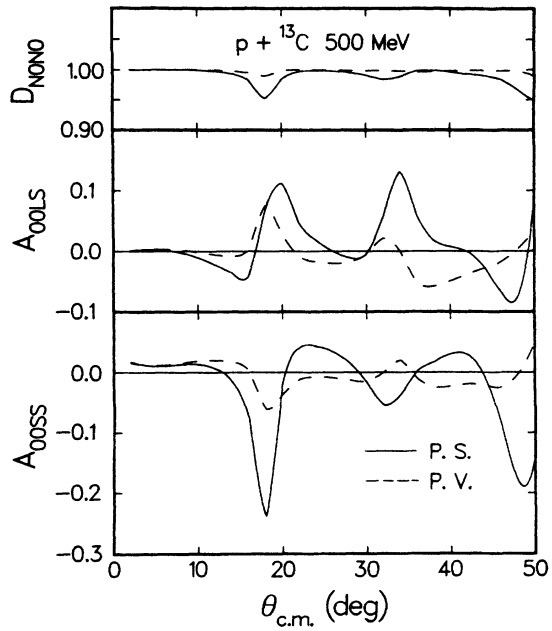

FIG. 15. Predicted differences in D_{NONO}, A_{00LS}, and A_{00SS} between pseudoscalar (solid curves) and pseudovector (dashed curves) coupling assuming the relativistic single particle lower component wave function of Eq. (23) for $\lambda_{1p_{1/2}}(r)$ as discussed in the text.

Sensitivity to the suppression of the effective valence nucleon isoscalar three-vector current for $\hat{n}$-target observables is, in the present model, similar to the sensitivity to $\lambda_{1p_{1/2}}(r)$ in the standard RIA calculations displayed in Fig. 10, since the isoscalar three-vector current makes the dominant contribution to these observables. Likewise, since the vector interaction contribution to D_{NONO} and the $\hat{s}$-target observables is minimal, little sensitivity to the core suppression of the isoscalar three-vector current is found for these cases.

Finally, a summary of the model predictions for D_{NONO} and several $\hat{n}$- and $\hat{s}$-target observables for $\vec{p}+{}^{13}\vec{C}$ at 500 MeV is exhibited in Fig. 16. The solid curves are results from the standard RIA calculation [i.e., RMFT $\varphi_{1p_{1/2}}(r)$ and $\lambda_{1p_{1/2}}(r)$ PS coupling]. Predictions obtained assuming pseudovector coupling with RMFT $\varphi_{1p_{1/2}}(r)$ and $\lambda_{1p_{1/2}}(r)$ from Eq. (23) are indicated by the dashed curves. Results using PS coupling and the quenched isoscalar three-vector current (RMFT values for $\varphi_{1p_{1/2}}$ and $\lambda_{1p_{1/2}}$) are shown by the dashed-dotted lines. Finally, the model results obtained assuming both pseudovector coupling and quenching of the isoscalar three-vector current [RMFT $\varphi_{1p_{1/2}}$ and $\lambda_{1p_{1/2}}$ of Eq. (23)] are given by the dotted curves. Comparison of these predictions with data would be very interesting and would challenge the underlying theoretical models and assumptions.

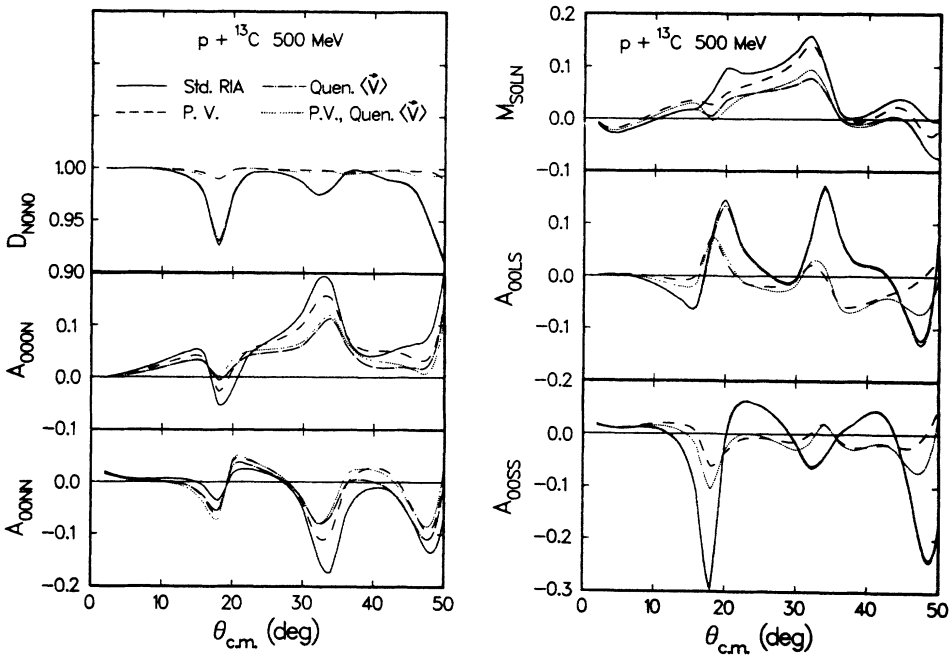

FIG. 16. Summary of the various predictions for D_{NONO}, A_{000N}, A_{00NN}, M_{S0LN}, A_{00LS}, and A_{00SS} for $\vec{p}+{}^{13}\vec{C}$ elastic scattering at 500 MeV assuming either the standard RIA model (solid curves), pseudovector coupling (dashed curves), core suppression of the isoscalar three-vector current (dashed-dotted curves), or both pseudovector coupling and core suppression of the isoscalar three-vector current (dotted curves) as discussed in the text.

IV. SUMMARY AND CONCLUSIONS

Because of increasing interest in spin degrees of freedom and relativistic effects in intermediate energy proton-nucleus scattering processes, and in anticipation of forthcoming experimental data[12] from polarized nuclear targets, the relativistic distorted wave Born approximation and the RIA model for the Lorentz invariant NN interaction were used to describe elastic scattering of polarized protons from a polarized odd-A nuclear target, specifically ^{13}C. Expressions for evaluating the $p+{}^{13}C$ elastic scattering amplitude were given where decomposition with respect to the individual Lorentz components of the NN effective interaction was emphasized. Modifications (to the standard RIA model of Refs. 1 and 2) which incorporate pseudovector coupling and quenching of the valence nucleon isoscalar three-vector current due to the response of the core nucleons to the presence of a single valence nucleon were also included.

The principal results of this study were the following: (1) the unpolarized target observables (except for D_{NONO}) are primarily sensitive to only the scalar and timelike vector portions of the core contribution to the scattering amplitude; (2) significant sensitivity to relativistic enhancement of $\lambda_{1p_{1/2}}(r)$ exists for most $\hat{n}$- and $\hat{s}$-target spin observables in the standard RIA model, but this sensitivity disappears when the theoretically motivated PV model with quenched isoscalar three-vector currents is used; (3) sensitivity to PV versus PS coupling is amply demonstrated in D_{NONO} and the $\hat{s}$-target observables; and (4) $\hat{n}$-target observables are dominated by the isoscalar three-vector current (spacelike vector contribution). Finally, a variety of predictions for several 500 MeV $\vec{p}+{}^{13}\vec{C}$ elastic scattering spin observables were given.

We conclude from this work that analyses of intermediate energy polarized proton elastic scattering data from lightweight, polarized nuclear targets should, in principle, provide a wealth of new information related to the following: (1) the Lorentz character of the NN effective interaction, (2) spin saturated core contributions to the total isoscalar three-vector current, (3) effective strengths and ranges of various parts of the NN interaction, and (4) possible relativistic binding potential enhancement of the lower component of the valence nucleon wave function. However, when faced with the analysis of actual $\vec{p}+{}^{13}\vec{C}$ elastic scattering data in the future it should be realized that the physics which must be ultimately dealt with in order to interpret the data is immensely complex, entailing most of the intermediate energy reaction dynamics known to be important and requiring very detailed relativistic and nonrelativistic nuclear structure calculations for a nucleus in a region of the periodic table whose properties are notoriously difficult to understand. Further progress in this theoretical investigation will most likely require (1) relativistic coupled channels calculation,[22] (2) sophisticated relativistic NN interaction models based on meson exchange theory, and (3) exchange, correlation, off-shell, and medium effects, etc. We hope that the interesting results obtained in this work will stimulate the theoretical community to address these and other problems.

ACKNOWLEDGMENTS

The authors would like to thank Dr. B. D. Serot for providing the RMFT wave functions and for many useful discussions and suggestions. Thanks is also given to Dr. J. R. Shepard for assistance in checking the numerical calculations and for helpful discussions. This research was supported in part by the U.S. Department of Energy, The Robert A. Welch Foundation, and The National Science Foundation.

*Present address: Theoretische Kernphysik, Universität Hamburg, Luruper Chaussee 149, 2000 Hamburg 50, Federal Republic of Germany.

[1]J. A. McNeil, J. Shepard, and S. J. Wallace, Phys. Rev. Lett. **50**, 1439 (1983); J. Shepard, J. A. McNeil, and S. J. Wallace, *ibid.* **50**, 1443 (1983); B. C. Clark, S. Hama, R. L. Mercer, L. Ray, and B. D. Serot, *ibid.* **50**, 1644 (1983).

[2]L. Ray and G. W. Hoffmann, Phys. Rev. C **31**, 538 (1985).

[3]M. V. Hynes, A. Picklesimer, P. C. Tandy, and R. M. Thaler, Phys. Rev. C **31**, 1438 (1985).

[4]G. W. Hoffmann *et al.*, Phys. Rev. Lett. **47**, 1436 (1981).

[5]D. A. Sparrow *et al.*, Phys. Rev. Lett. **54**, 2207 (1985); J. Piekarewicz, R. D. Amado, and D. A. Sparrow, Phys. Rev. C **32**, 949 (1985).

[6]M. L. Barlett, G. W. Hoffmann, and L. Ray, Phys. Lett. **158B**, 289 (1985).

[7]S. K. Nanda *et al.*, Phys. Rev. Lett. **51**, 1526 (1983); Rutgers University Report RU8664, 1986.

[8]Proceedings of the LAMPF Workshop on Physics with Polarized Nuclear Targets, Los Alamos National Laboratory, LAMPF Conference Report LA-10772-C 1986, edited by G. Burleson, W. Gibbs, G. Hoffmann, J. J. Jarmer, and N. Tanaka.

[9]L. Ray *et al.*, Phys. Rev. Lett. **56**, 2465 (1986).

[10]See the articles in Ref. 8 by D. Hill, p. 24, and M. Krumpolc, p. 38.

[11]J. J. Jarmer *et al.*, Nucl. Instrum. Methods **A250**, 576 (1986).

[12]See the following Los Alamos Meson Physics Facility experimental proposals: EXP: 955, spokesmen: G. W. Hoffmann, R. L. Ray, M. L. Barlett, and J. J. Jarmer; EXP: 1025, spokesmen: G. R. Burleson and D. Dehnhard; EXP 1023, spokesmen: J. Comfort and G. Kyle.

[13]J. R. Shepard, E. Rost, and J. Piekarewicz, Phys. Rev. C **30**, 1604 (1984).

[14]See the article in Ref. 8 by J. Shepard, p. 73.

[15]J. A. McNeil, L. Ray, and S. J. Wallace, Phys. Rev. C **27**, 2123 (1983).

[16]C. J. Horowitz, Phys. Rev. C **31**, 1340 (1985).

[17]J. A. Tjon and S. J. Wallace, Phys. Rev. C **32**, 1667 (1985).

[18]S. J. Seestrom-Morris *et al.*, Phys. Rev. C **30**, 270 (1984).

[19]R. J. Furnstahl and B. D. Serot, Nucl. Phys. **A468**, 539 (1987).

[20]J. A. McNeil *et al.*, Phys. Rev. C **34**, 746 (1986).

[21]C. J. Horowitz and B. D. Serot, Nucl. Phys. **A368**, 503 (1981). The valence neutron wave function from this work is actually the $1p_{1/2}$ single particle eigenstate of the ^{12}C relativistic Hartree binding potential.

[22]A coupled channels, Dirac equation computer program capable of handling the $\vec{p}+^{13}\vec{C}$ scattering problem is currently being developed by one of us (R.L.M.).

[23]L. Ray, G. S. Blanpied, W. R. Coker, R. P. Liljestrand, and G. W. Hoffmann, Phys. Rev. Lett. **40**, 1547 (1978).

[24]S. Cohen and D. Kurath, Nucl. Phys. **73**, 1 (1965).

[25]M. K. Singham and F. Tabakin, Phys. Rev. C **34**, 637 (1986).

[26]J. A. Tjon and S. J. Wallace, Phys. Rev. C **35**, 280 (1987); **32**, 267 (1985).

[27]D. P. Murdock and C. J. Horowitz, Phys. Rev. C **35**, 1442 (1987).

[28]J. D. Lumpe and L. Ray, Phys. Rev. C **35**, 1040 (1987).

[29]B. C. Clark *et al.*, Phys. Rev. Lett. **51**, 1808 (1983).

[30]See the article in Ref. 8 by L. Ray, p. 41.

[31]J. A. Tjon and S. J. Wallace, Phys. Rev. C **36**, 1085 (1987); S. J. Wallace and N. Ottenstein, private communication.

[32]L. D. Miller, Ann. Phys. (N.Y.) **91**, 40 (1975).

[33]B. D. Serot and J. D. Walecka, in *Advances in Nuclear Physics*, edited by J. W. Negele and E. Vogt (Plenum, New York, 1986), Vol. 16.

[34]J. R. Shepard, E. Rost, C. Y. Cheung, and J. A. McNeil, University of Colorado Report NPL-1029, 1987; J. R. Shepard, private communication.

[35]J. Bystricky, F. Lehar, and P. Winternitz, J. Phys. (Paris) **39**, 1 (1978).

[36]R. A. Arndt, J. S. Hyslop III, and L. D. Roper, Phys. Rev. D **35**, 128 (1987); R. A. Arndt *et al.*, *ibid.*, **28**, 97 (1983).

[37]I. Sick and J. S. McCarthy, Nucl. Phys. **A150**, 631 (1970).

[38]L. Ray, Phys. Rev. C **19**, 1855 (1979).

[39]W. Bertozzi, J. Friar, J. Heisenberg, and J. W. Negele, Phys. Lett. **41B**, 408 (1972).

[40]J. Dechargé and D. Gogny, Phys. Rev. C **21**, 1568 (1980); J. Dechargé, M. Girod, D. Gogny, and B. Grammaticos, Nucl. Phys. **A358**, 203c (1981); J. Dechargé, private communication.

[41]G. W. Hoffmann *et al.* (unpublished).

[42]E. E. van Faassen and J. A. Tjon, Phys. Rev. C **30**, 285 (1984).

[43]B. C. Clark, S. Hama, and R. L. Mercer, in *The Interaction Between Medium Energy Nucleons in Nuclei (Indiana Cyclotron Facility, Bloomington, Indiana)*, Proceedings of the Workshop on the Interactions Between Medium Energy Nucleons in Nuclei, edited by H. O. Meyer, AIP Conf. Proc. No. **97** (AIP, New York, 1982), p. 260.

[44]Two-parameter Fermi function fits to the relativistic Hartree potentials for ^{12}C yield values of V_S, c_S, z_S, V_V, c_V, and z_V of -431.1 MeV, 2.405 fm, 0.5079 fm, 400.3 MeV, 2.264 fm, and 0.4955 fm, respectively. The $1p_{1/2}$ lower component wave function and subsequent $\vec{p}+^{13}\vec{C}$ scattering observables obtained from the use of these potential parameters in Eqs. (23) and (24) are negligibly different from the results shown in the text.

[45]R. J. Glauber and P. Osland, Phys. Lett. **80**, 401 (1979).